

Persistent Sodium Current, Membrane Properties and Bursting Behavior of Pre-Bötzinger Complex Inspiratory Neurons In Vitro

CHRISTOPHER A. DEL NEGRO,^{1,*} NAOHIRO KOSHIYA,^{1,2,*} ROBERT J. BUTERA, JR.,³ AND JEFFREY C. SMITH¹

¹Cellular and Systems Neurobiology Section, Laboratory of Neural Control, National Institute of Neurological Disorders and Stroke, National Institutes of Health, Bethesda, Maryland 20892-4455; ²Blanchette Rockefeller Neurosciences Institute, Rockville, Maryland 20850-3332; and ³Laboratory for Neuroengineering, Institute for Bioengineering and Biosciences, Georgia Institute of Technology, Atlanta, Georgia 30332

Received 6 February 2002; accepted in final form 22 July 2002

Del Negro, Christopher A., Naohiro Koshiya, Robert J. Butera, Jr., and Jeffrey C. Smith. Persistent sodium current, membrane properties and bursting behavior of pre-Bötzinger complex inspiratory neurons in vitro. *J Neurophysiol* 88: 2242–2250, 2002; 10.1152/jn.00081.2002. We measured persistent Na⁺ current and membrane properties of bursting-pacemaker and nonbursting inspiratory neurons of the neonatal rat pre-Bötzinger complex (pre-BötC) in brain stem slice preparations with a rhythmically active respiratory network in vitro. In whole-cell recordings, slow voltage ramps (≤ 100 mV/s) inactivated the fast, spike-generating Na⁺ current and yielded N-shaped current-voltage relationships with nonmonotonic, negative-slope regions between -60 and -35 mV when the voltage-sensitive component was isolated. The underlying current was a TTX-sensitive persistent Na⁺ current (I_{NaP}) since the inward current was present at slow voltage ramp speeds (3.3–100 mV/s) and the current was blocked by 1 μM TTX. We measured the biophysical properties of I_{NaP} after subtracting the voltage-insensitive “leak” current (I_{Leak}) in the presence of Cd²⁺ and in some cases tetraethylammonium (TEA). Peak I_{NaP} ranged from -50 to -200 pA at a membrane potential of -30 mV. Decreasing the speed of the voltage ramp caused time-dependent I_{NaP} inactivation, but this current was present at ramp speeds as low as 3.3 mV/s. I_{NaP} activated at -60 mV and obtained half-maximal activation near -40 mV. The subthreshold voltage dependence and slow inactivation kinetics of I_{NaP} , which closely resemble those of I_{NaP} mathematically modeled as a burst-generation mechanism in pacemaker neurons of the pre-BötC, suggest that I_{NaP} predominantly influences bursting dynamics of pre-BötC inspiratory pacemaker neurons in vitro. We also found that the ratio of persistent Na⁺ conductance to leak conductance ($g_{\text{NaP}}/g_{\text{Leak}}$) can distinguish the phenotypic subpopulations of bursting pacemaker and nonbursting inspiratory neurons: pacemaker neurons showed $g_{\text{NaP}}/g_{\text{Leak}} > g_{\text{NaP}}/g_{\text{Leak}}$ in nonpacemaker cells ($P < 0.0002$). We conclude that I_{NaP} is ubiquitously expressed by pre-BötC inspiratory neurons and that bursting pacemaker behavior within the heterogeneous population of inspiratory neurons is achieved with specific ratios of these two conductances, g_{NaP} and g_{Leak} .

INTRODUCTION

The neural rhythm for breathing in mammals is generated by a network in the brain stem. The intrinsic membrane and synaptic properties of constituent neurons in this network determine the mechanism of rhythm generation. Here we quan-

tify biophysical properties of inspiratory neurons in the pre-Bötzinger complex (pre-BötC)—the critical locus for rhythm generation in the ventrolateral medulla that contains the neurons that are necessary and sufficient to generate inspiratory motor rhythms in vitro (Rekling and Feldman 1998; Smith et al. 1991, 2000) and in vivo (Koshiya and Guyenet 1996; Ramirez et al. 1998) and are required for normal breathing in intact awake adult rats in vivo (Gray et al. 2001). The pre-BötC contains a subset of inspiratory neurons that express autonomous oscillatory bursting behavior, i.e., “pacemaker” neurons (Johnson et al. 1994; Koshiya and Smith 1999a; Smith et al. 1991; Thoby-Brisson and Ramirez 2001) as well as nonbursting neurons. Rhythm generation does not require chloride-mediated postsynaptic inhibition (Feldman and Smith 1989; Gray et al. 1999) and inspiratory neuron activity is synchronized via excitatory synapses (Koshiya and Smith 1999a). Therefore we proposed that an excitatory network of pre-BötC neurons putatively constitutes the rhythm-generating kernel and that rhythm emerges at the population level from a dynamic interaction of intrinsic cellular properties and excitatory network synaptic interactions (Butera et al. 1999b; Smith et al. 2000).

Previously we modeled pre-BötC inspiratory neurons and hypothesized that a persistent Na⁺ current (I_{NaP}) interacting with a K⁺-dominated, voltage-insensitive leak-type current (I_{Leak}) can give rise to bursting pacemaker behavior in a subset of cells with appropriate levels of the key conductances—the persistent Na⁺ conductance (g_{NaP}) and the leak conductance (g_{Leak}) (Butera et al. 1999a). We then assembled a heterogeneous network model of the pre-BötC kernel containing bursting-pacemaker and nonbursting phenotypes (Butera et al. 1999b). The relative magnitudes of g_{NaP} and g_{Leak} determines whether model neurons exhibit bursting-pacemaker or nonbursting behavior when other biophysical properties are kept constant. Heterogeneity of g_{NaP} and g_{Leak} was shown in the models to importantly affect network dynamic behavior, and parameter distributions were originally chosen to optimize network performance. Recently, in vitro experiments verified that the models can closely resemble neuronal and network behaviors recorded in vitro (Del Negro et al. 2001). However,

*C. A. Del Negro and N. Koshiya contributed equally to this study.

Address for reprint requests: J. C. Smith, 49 Convent Drive, Room 3A50, Bethesda, MD 20892-4455 (E-mail: jsmith@helix.nih.gov).

The costs of publication of this article were defrayed in part by the payment of page charges. The article must therefore be hereby marked “advertisement” in accordance with 18 U.S.C. Section 1734 solely to indicate this fact.

several issues remain unresolved. If neonatal rat pre-BötC pacemaker neurons express I_{NaP} , then 1) what are its biophysical properties? and 2) how much heterogeneity is there in the magnitude of g_{NaP} ? Also, what intrinsic membrane parameters engender bursting pacemaker behavior in the subset of inspiratory neurons expressing these properties? In particular, 3) are the relative magnitudes of g_{NaP} and g_{Leak} related to bursting pacemaker and nonbursting behaviors, as demonstrated in the models?

To address these questions we sampled inspiratory neurons using whole-cell patch-clamp recordings in the pre-BötC of neonatal rat thin brain stem slices *in vitro*. We determined that I_{NaP} is expressed in all inspiratory neurons that we sampled, both bursting pacemaker and nonbursting inspiratory cells, but that I_{NaP} engenders bursting according to the relative magni-

tude of g_{NaP} and g_{Leak} . We also examined the heterogeneity of membrane properties and thus obtained information on the distribution of inspiratory neuron properties within the pre-BötC. Preliminary reports of this work have appeared in abstract form (Koshiya and Smith 1999b; Koshiya et al. 2001).

METHODS

In vitro brain stem slice preparation

Thin transverse slices (350- μ m thick, Fig. 1A) containing the pre-BötC were cut from the medulla of neonatal rats (P0–P3) in artificial cerebrospinal fluid (ACSF) containing (in mM) 128.0 NaCl, 3.0 KCl, 1.5 CaCl₂, 1.0 MgSO₄, 21.0 NaHCO₃, 0.5 NaH₂PO₄, and 30.0 D-glucose, equilibrated with 95% O₂-5% CO₂ (27°C, pH 7.4), as originally described (Smith et al. 1991). Slices were cut to expose the

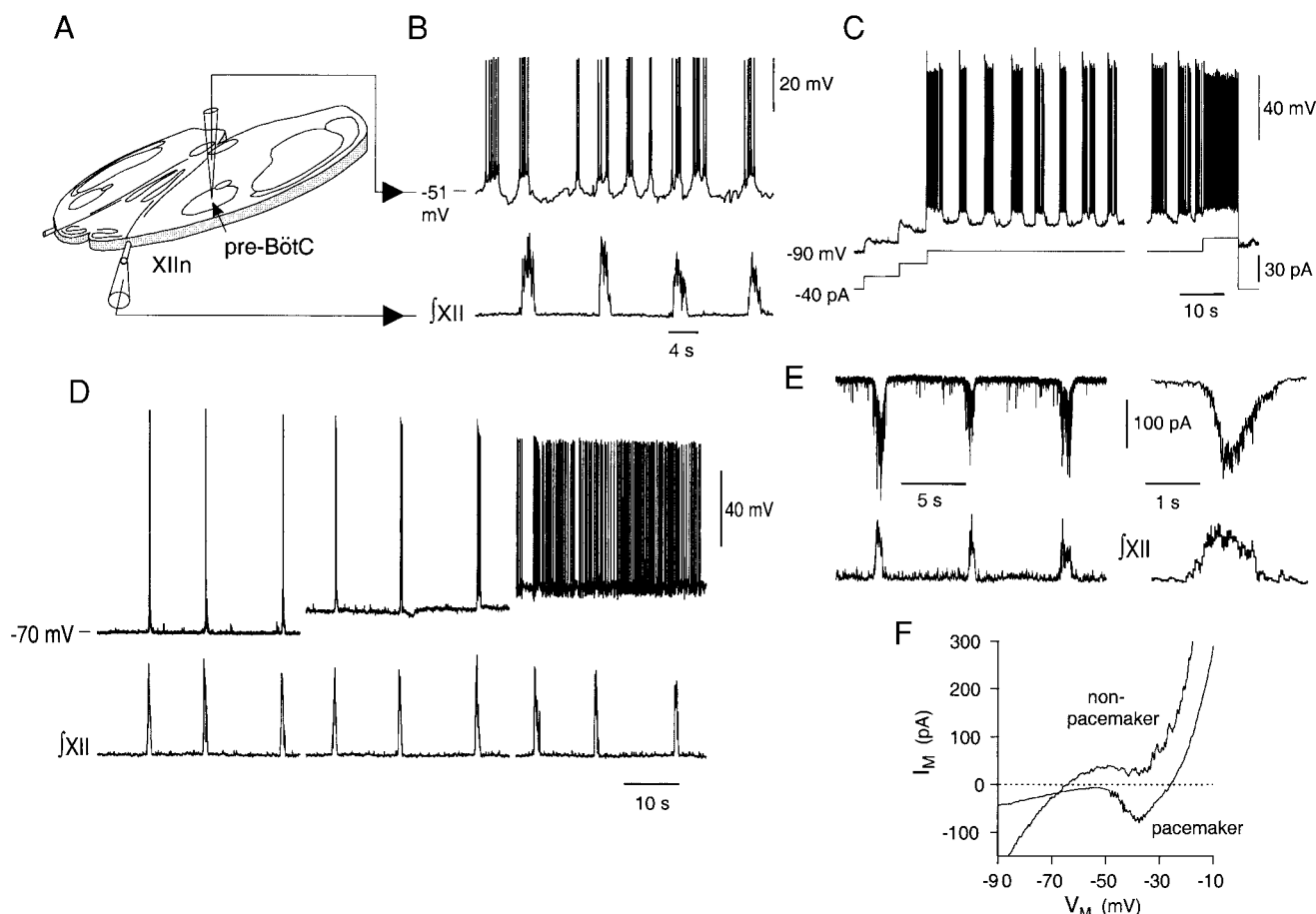


FIG. 1. Activity patterns of bursting pacemaker and nonpacemaker phenotype inspiratory neurons recorded in the pre-BötC. *A*: experimental configuration for whole-cell recording of inspiratory neurons in pre-BötC and extracellular recording of network activity from hypoglossal nerve (XIIIn) with motoneuron population discharge (\int XII) in thin (300–350 μ m) medullary slice preparations. Whole-cell recordings of visualized neurons were obtained from the caudal end of the pre-BötC exposed on the cut surface of slice. *B* and *C*: inspiratory pacemaker neurons at depolarized membrane potentials exhibit ectopic oscillatory bursts between phases of inspiratory discharge with network activity intact (*B*) and exhibit intrinsic voltage-dependent oscillatory bursting (*C*) at depolarized membrane potentials when network activity and synaptic transmission is blocked. Pacemaker neurons exhibit multistate activity patterns (quiescence, oscillatory bursting, and tonic spiking) as baseline V_M is depolarized under current clamp. *D*: nonpacemaker inspiratory neurons exhibit rhythmic synaptic drive potentials and spike discharge in phase with XIIIn discharge and only tonic spiking (without ectopic bursting between inspiratory phase discharge) at depolarized baseline V_M (see text). *E*: example of inspiratory synaptic drive currents measured under voltage clamp at -70 mV. Area of the synaptic current envelope (see fast time base trace at right) was measured to quantify synaptic charge transfer presented in Fig. 2. *F*: examples of current-voltage (I - V) relationships of bursting pacemaker and nonpacemaker inspiratory cell phenotypes in *C* and *D*, respectively, generated by slow voltage-clamp ramps (30 mV/s) under conditions in which synaptic transmission is blocked by low Ca^{2+} solution and 200 μ M Cd^{2+} . Both types of inspiratory neurons show inward current with a negative slope region in I - V relationship above -60 mV V_M .

caudal surface of the pre-BötC (Koshiya and Smith 1999a). Low calcium solution used in some experiments contained 124.5 mM NaCl, 3.0 mM KCl, 0.5 mM CaCl₂, 2.0 mM MgCl₂, 25.0 mM NaHCO₃, 30.0 mM D-glucose, and 100–200 μM CdCl₂. Tetraethylammonium chloride (TEA, 20 mM) was substituted on an equimolar basis for NaCl for some experiments to attenuate K⁺ currents. TTX (Sigma) was bath applied at 1 μM and 6-cyano-7-nitroquinoxaline-2,3-dione disodium (CNQX, Sigma) was applied at 10–20 μM.

The slice was stabilized with the caudal surface up using a platinum ring anchor with nylon fibers (Edwards et al. 1989) in an approximately 0.5-ml recording chamber mounted on a fixed-stage videomicroscope (Zeiss Axioskop FS-1) with infrared-differential interference contrast (IR-DIC) optics and perfused with ACSF at 2–4 ml/min. These slices containing the pre-BötC, premotor circuits, and hypoglossal respiratory motoneurons spontaneously generate rhythmic inspiratory motor discharge that can be recorded from the hypoglossal (XII) nerve rootlets (also captured in the slice) (Smith et al. 1991) and maintained for ≥24 h by raising the ACSF K⁺ concentration ([K⁺]_o) to 7–9 mM. XII inspiratory bursts were recorded using fire-polished glass suction electrodes (40–90 μm ID) and a differential amplifier (Cyberamp 360, Axon Instruments) with variable gain and a 0.3–1 kHz band-pass filter. XII activity was rectified and integrated (JXII) with either an analog integrator or digitally with Chart software (ADInstruments).

Calcium imaging for functional identification of rhythmic pre-BötC neurons

In some experiments rhythmically active inspiratory neurons in the pre-BötC were first identified for whole-cell patch-clamp recording using Ca²⁺ imaging of neuron activity, as previously described in detail (Koshiya and Smith 1999a). Briefly, Calcium Green-1 AM (Molecular Probes) (CaG; 50 μg) dissolved in 5 μl of DMSO containing 25 μg of pluronic F-127 (BASF) and dispersed in 10 μl of ACSF was injected with a glass pipette (approximately 10-μm tip diam) into the slice near the midline to retrogradely label pre-BötC neurons. After 8–12 h, CaG fluorescence labeled inspiratory neurons were visualized in the pre-BötC with a 75-W xenon epilluminator, optical filters (excitation 485 nm, emission 530 nm, 505 nm beam splitter, Omega Optical), and a CCD camera with image intensifier (ICCD-1000F, VideoScope International).

Electrophysiological recording

Whole-cell patch-clamp recordings were obtained with an EPC-9 amplifier (version C, HEKA). Electrodes were fabricated from capillary glass (1.5 mm OD, 0.87 mm ID, resistance 4–7 MΩ). Electrodes were filled with solution containing the following (in mM): 136.0 K-gluconate, 4.0 KCl, 10.0 HEPES, 4.0 Mg-ATP, 0.3 Na-GTP, and 2.0 sodium phosphocreatine, pH 7.3, or, for some experiments, 130.0 K-gluconate, 10 Na-gluconate, 4.0 NaCl, 10.0 HEPES, 4.0 Mg-ATP, 0.3 Na-GTP, and 4.0 sodium phosphocreatine, pH 7.3. A liquid junction potential of 8 mV was corrected off-line. Series resistance compensation was applied via the EPC-9. Intracellular data were acquired digitally at 10 kHz and combined with raw XII and integrated XII inspiratory activity acquired at 4 kHz using Pulse (HEKA) and Chart v4.0 (ADInstruments).

Data analysis

Cell capacitance (C_M) was determined from the integral of the transient capacity current (I_C , leak subtracted) evoked by a series of 15-ms hyperpolarizing voltage-step commands applied within –10 mV of resting potential, using $\int I_C = Q_M$ at each command potential (V_M). C_M is determined from the slope of the plot of Q_M versus ΔV_M for the series of step commands. Input resistance (R_M) was determined via linear regression applied to the linear portion of the quasi-steady-

state current-voltage (I - V) relationship generated by a slow voltage ramp (30 mV/s) initiated from –90 mV. In subsequent analyses we take the reciprocal of R_M as an estimate of the voltage-insensitive leak conductance (g_{Leak} e.g., see Fig. 4). Series resistance (R_S) was calculated from the decay-time constant of I_C , since in voltage clamp $\tau \cong R_S C_M$, where τ is an exponential fit to the I_C decay time. In general an adequate voltage-clamp requires $R_M \geq 10 R_S$. Cells failing to meet this criterion were excluded from voltage-clamp analysis.

Voltage dependence and kinetics of whole-cell currents were analyzed from voltage-clamp data using Pulsefit (HEKA), Chart (ADInstruments), and Igor Pro (Wavemetrics) software. Regression analyses were performed with a nonlinear least-squares method in IDL (Research Systems) or Igor Pro. Voltage-ramp data were fit to Boltzmann functions: $g/g_{max} = [1 + \exp((V_M - V_{1/2})/k)]^{-1}$, where g and g_{max} represent whole-cell conductance at V_M and the maximal conductance (for all V_M), respectively. V_M is membrane potential, $V_{1/2}$ is the voltage for half-maximal activation, and k is a slope factor. Kolmogorov–Smirnov tests were performed with Igor Pro. Monte Carlo-based statistical analyses were performed using Igor Pro and Resampling Statistics v5. Normality of data distributions was tested by a Shapiro–Wilk test (JMP software, SAS Institute).

RESULTS

Electrophysiological phenotypes of pre-BötC inspiratory neurons

The thin brain stem slice preparations (Fig. 1A) spontaneously generate rhythmic inspiratory motor discharge from the XII nerve rootlets (shown as upward deflections of the integrated XII activity in Fig. 1, B and D), allowing respiratory cells to be identified in the context of network activity. We recorded 71 inspiratory neurons in the pre-BötC using whole-cell patch-clamp techniques. These cells were identified based on membrane depolarization or intracellular Ca²⁺ transients (Koshiya and Smith 1999a) during the inspiratory phase. Shifting the membrane potential (V_M) under current clamp revealed voltage-dependent intrinsic bursting behavior in a subset of inspiratory neurons ($n = 22$) defined as bursting-pacemaker cells (also see Koshiya and Smith 1999a; Smith et al. 1991; Thoby-Brisson and Ramirez 2001). At baseline V_M of approximately –50 mV or greater, pacemaker neurons generated ectopic bursts during the interval between inspiratory phases of network activity (Fig. 1B). Nonbursting inspiratory neurons ($n = 49$) discharged bursts of action potentials only during the inspiratory phase due to excitatory inspiratory synaptic drive. In contrast to pacemaker-type cells, these cells generated only tonic spiking without ectopic bursts between the phases of synaptically driven inspiratory discharge when the baseline V_M was depolarized above –50 mV (Fig. 1D).

To examine intrinsic behavior of isolated inspiratory cells, we blocked excitatory synaptic transmission using CNQX (Koshiya and Smith 1999a) or blocked all chemical synaptic transmission using low Ca²⁺ solution (with elevated Mg²⁺ and 100–200 μM Cd²⁺ to block voltage-dependent Ca²⁺ channels). Either method stopped respiratory network activity and blocked rhythmic excitatory synaptic drive currents to inspiratory pre-BötC neurons as assessed under voltage clamp.

Bursting behavior in inspiratory pacemaker neurons was voltage dependent, as previously shown (Del Negro et al. 2001; Koshiya and Smith 1999a; Smith et al. 1991; Thoby-Brisson and Ramirez 2001). To confirm that our sample of inspiratory pacemaker neurons exhibited intrinsic voltage-dependent

bursting, we progressively depolarized cells in current clamp in the absence of network activity and phasic synaptic drive (Fig. 1C). Depolarizing bias current application caused cells to move from quiescence at hyperpolarized potentials to bursting, where the cells alternate between phases of rapid subthreshold depolarization with spike discharge (i.e., bursts), followed by repolarization and quiescence. Cells transitioned to the tonic spiking state at highly depolarized levels (above approximately -45 mV). Nonbursting inspiratory cells subjected to similar protocols progressed from quiescence to steady tonic spiking as baseline V_M was progressively depolarized (not shown) (Thoby-Brisson and Ramirez 2001).

Distribution of membrane and synaptic properties in inspiratory neurons

We used voltage-clamp protocols before and after blocking synaptic transmission to analyze the intrinsic membrane and synaptic properties of pre-BötC inspiratory neurons. Voltage-ramp commands were used to measure the quasi-steady-state I - V relationship with a ramp speed of ≤ 100 mV/s (see Figs. 1, 3, and 4). All inspiratory neurons examined showed nonmonotonic N-shaped I - V curves (e.g., Fig. 1F) with the negative slope region at potentials above -60 mV under the slow voltage ramps after subtraction of the “leak” current (below), suggesting the presence of a common non- or slowly inactivating inward current in these cells.

We assessed the basic properties of our sample from the inspiratory cell population, using input resistance (R_M), whole-cell capacitance (C_M), peak inward current (I_{peak} , measured between -40 and -30 mV in the quasi-steady-state I - V curve, see Figs. 1F, 3A, and 4, A and B), and synaptic charge transfer (Q_{syn}) computed from the integral of rhythmic inspiratory drive currents measured under voltage clamp (below). These mea-

surements are displayed in histograms for the pooled sample in Fig. 2 (top) and as cumulative probability histograms that compare bursting pacemaker and nonbursting inspiratory neuron phenotypes (bottom).

The distributions are skewed for R_M , I_{peak} , and Q_{syn} , with most cells clustering below sample means (Fig. 2). Therefore we compared R_M , C_M , I_{peak} , and Q_{syn} between pacemaker and nonpacemaker phenotypes using a nonparametric Kolmogorov–Smirnov test. Except C_M , which showed a statistical difference in distributions between the phenotypes (pacemaker or not, $P < 0.01$), all other properties (R_M , I_{peak} , and Q_{syn}) distributed indistinguishably between the phenotypes and were therefore pooled for further analyses. R_M , I_{peak} , and Q_{syn} showed significant deviation from normal distributions ($P < 0.05$, Shapiro–Wilks test). Mean pooled R_M was 380 ± 32 M Ω : pacemaker neurons ($n = 20$) had a mean R_M of 430 ± 56 M Ω and nonpacemaker cells had a mean R_M of 348 ± 40 M Ω ($n = 32$) (Fig. 2A), which was not statistically different. C_M was significantly different between pacemaker ($n = 21$) and nonpacemaker ($n = 29$) cells: 32 ± 3 versus 48 ± 3 pF, respectively ($P < 0.01$). The pooled sample mean for I_{peak} , which measures the peak persistent inward current (after leak current subtraction) in the quasi-steady-state I - V curve, was 118 ± 23 pA (Fig. 2C) ($n = 9$ pacemaker cells, 30 nonpacemaker cells).

Q_{syn} was computed from the integral of the envelope of inspiratory drive currents (I_{syn}) (see Fig. 1E) measured under voltage clamp at $V_M = -70$ mV. I_{syn} was collected for five or more cycles and averaged. Q_{syn} was 11.6 ± 3.0 pC for pacemaker cells ($n = 11$) and 12.8 ± 2.0 pC for nonpacemaker neurons ($n = 28$), which was not significantly different between phenotypes ($P = 0.75$). The pooled sample mean was 12.4 ± 2.0 pC for Q_{syn} (Fig. 2D).

These results suggested that inspiratory bursting-pacemaker

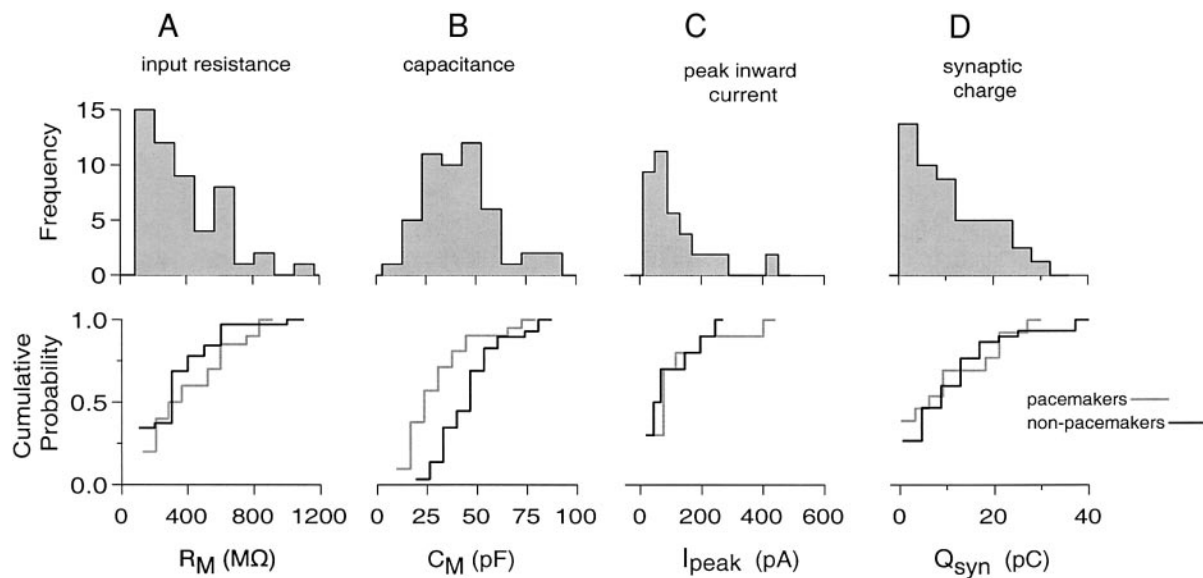


FIG. 2. Membrane properties of sampled bursting pacemaker and nonpacemaker inspiratory populations. A–D: histograms of pooled sample of pacemaker and nonpacemaker inspiratory populations (top) and separate cumulative probability histograms (bottom) of membrane input resistance (R_M), whole-cell capacitance (C_M), peak inward current (I_{peak} , measured between -40 and -30 mV on the quasi-steady-state I - V curve), and synaptic charge transfer (Q_{syn} computed from the integral of rhythmic inspiratory drive currents measured under voltage clamp at -70 mV). Pooled population distributions were positively skewed for R_M , I_{peak} , and Q_{syn} , with most neurons clustering below sample means. Differences in separate population means were not significant, except for C_M (see text for full explanation).

and nonpacemaker neurons cannot be reliably distinguished by any single intrinsic parameter, other than C_M .

Persistent Na^+ current in pre-BötC inspiratory neurons

Inspiratory pacemaker neurons in neonatal rat slices depend on a persistent Na^+ current (I_{NaP}), since bursting continues in low Ca^{2+} solution (Del Negro et al. 2001; Johnson et al. 1994) and bursting ceases in the presence of TTX (Thoby-Brisson and Ramirez 2001). Here, we tested for the presence of I_{NaP} in neonatal rat inspiratory pacemaker neurons using a voltage-clamp ramp protocol ($n = 9$ neurons tested) with ramps generated over the voltage interval -80 to $+10$ mV with ramp speeds that were slow enough (≤ 100 mV/s) in some neurons to maintain space clamp sufficiently to prevent activation of the transient fast action potential-generating Na^+ current (see Fig. 4A). We identified bursting pacemaker-type inspiratory neurons based on ectopic bursts in the context of network activity (e.g., Fig. 1B) (Del Negro et al., 2001; Koshiya and Smith 1999a) and then isolated the cells for voltage-clamp analysis in low Ca^{2+} solution containing Cd^{2+} (100 – 200 μM) to block chemical synaptic transmission and voltage-dependent Ca^{2+} currents. The inward current in the quasi-steady-state I - V curve was completely blocked by 1 μM TTX (Fig. 3A), indicating the presence of a TTX-sensitive I_{NaP} , obtained by subtraction of I - V curves.

To characterize the voltage dependence of activation, we fitted a Boltzmann function (see METHODS) to conductance-voltage data (Fig. 3B and see Fig. 4D), where the conductance was calculated from the I - V relationships and a Na^+ reversal potential of $+50$ mV (based on bathing and pipette solutions). I_{NaP} was consistently ($n = 9$ pacemaker neurons) activated starting at -60 mV and reached half-maximal activation at approximately -40 mV, with a slope factor k of approximately 5 (e.g., Fig. 3, B and C, Fig. 4D). Since all inspiratory neurons examined exhibited an N-shaped, quasi-steady-state I - V relationship with a negative-slope region with similar voltage dependence, we hypothesized that I_{NaP} was commonly expressed in all inspiratory cells. Therefore we applied TTX to

nonbursting inspiratory neurons ($n = 4$) and obtained identical results. TTX blocked the subthreshold-activating inward current, and activation curves for the subtracted current (I_{NaP}) fitted with a Boltzmann function for nonbursting inspiratory neurons were indistinguishable from those obtained for pacemaker cells (Fig. 3, B and C).

Ramp-rate dependence of I_{NaP}

Using the voltage-clamp ramp protocol, we quantified the voltage-activated inward membrane current in three pacemaker-type neurons at different ramp speeds (e.g., 100, 33, 10, and 3.3 mV/s, Fig. 4) under conditions in which Ca^{2+} currents were blocked with Cd^{2+} (100 – 200 μM). The voltage-activated inward current was extracted (Fig. 4A, solid curve) by subtracting the passive leak current I_{Leak} , extrapolated from linear regression fits to the I - V curve at membrane voltages between -80 and -60 mV. Consistent with the I - V relationships obtained from the TTX protocol, the inward current activated at approximately -60 mV. The multispeed voltage ramp protocol revealed that the amplitude of this inward current was attenuated progressively at slower ramp speeds (Fig. 4, B and C), reflecting the slow inactivation kinetics of I_{NaP} . The conductance corresponding to each current was calculated using the Na^+ reversal potential ($+50$ mV) and normalized to the peak conductance to compare activation characteristics at different ramp rates. The normalized activation characteristic relationship was essentially identical for different ramp speeds over the membrane voltage range -80 to -30 mV. A single Boltzmann function fitted to the data set from one of the neurons (not shown) gave a $V_{1/2}$ of -44.7 mV and $k = -4.4$ mV, similar to the values obtained for the two other pacemaker cells studied with this protocol and similar to values obtained for the TTX-sensitive I_{NaP} described above.

I_{NaP} was further isolated in two pre-BötC pacemaker cells with K^+ conductances blocked with TEA, in addition to Ca^{2+} conductances blocked with Cd^{2+} (Fig. 4C), to minimize voltage-dependent outward K^+ currents and distortion of the ramp I - V relationship. Similar to the voltage-clamp data obtained

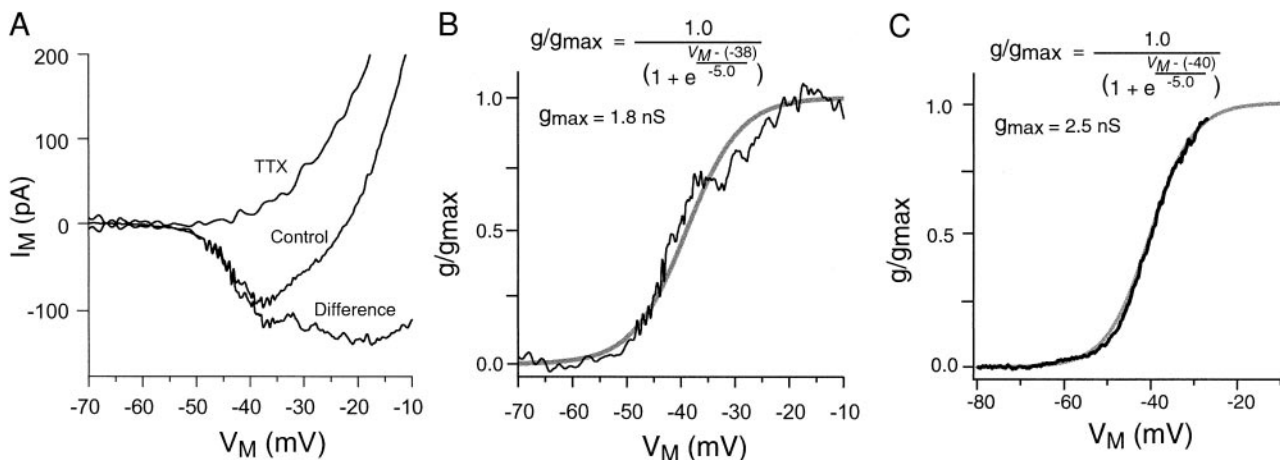


FIG. 3. TTX sensitivity of persistent inward current in bursting pacemaker inspiratory neurons. A: inward current and negative slope region of ramp (30 mV/s) I - V relationship (control) is completely blocked by 1 μM TTX in the neuron illustrated. Difference curve yields I - V relationship for persistent inward current. B and C: Boltzmann functions (thick gray curves, equations and parameters given) fitted to conductance-voltage relationships derived from difference I - V relationships are essentially identical for bursting pacemaker and nonpacemaker inspiratory cells. For the nonpacemaker inspiratory neuron shown in C, plateau inward currents were not obtained at membrane voltages above -30 mV.

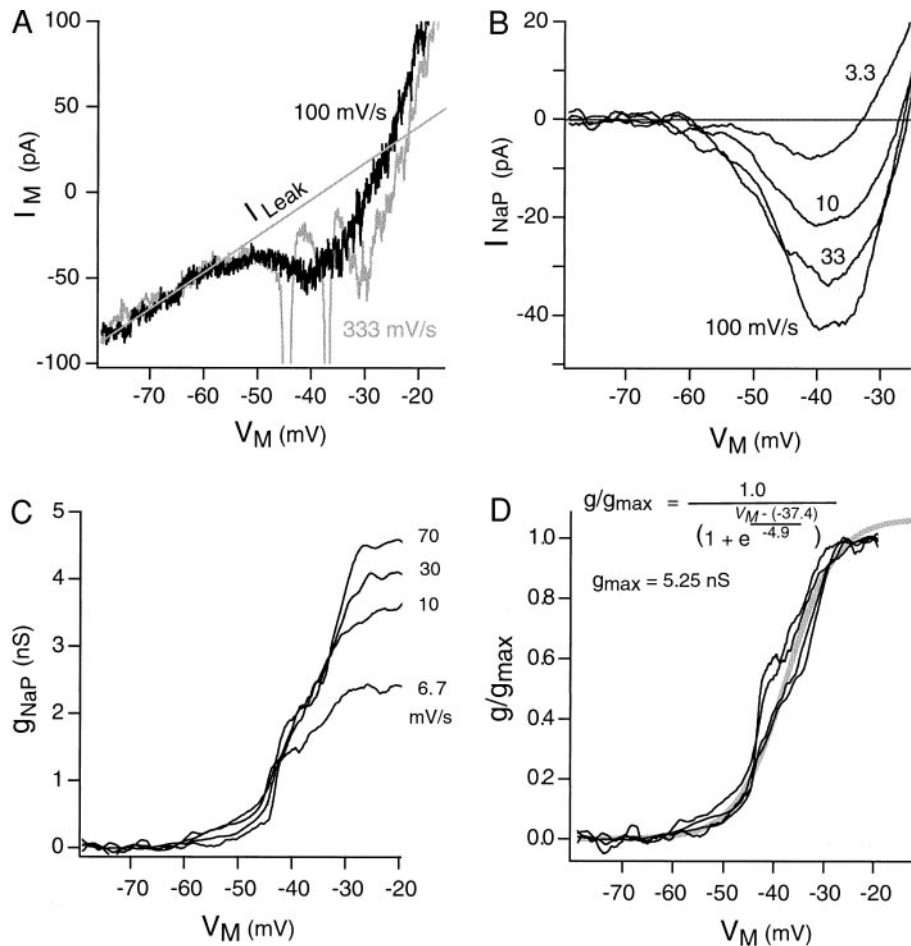


FIG. 4. Persistent sodium conductance (g_{NaP}) in inspiratory pacemaker neurons of pre-BötC. *A* and *B*: isolation of persistent current from total membrane currents in the presence of $100 \mu\text{M}$ Cd^{2+} . Transient, unclamped action potential-generating Na^+ current (downward spikes in *A*) observed in a fast voltage ramp (333 mV/s) is suppressed at slower ramp speed (100 mV/s , *A*). Voltage-insensitive leak current (I_{Leak}) is characterized from the linear portion of the membrane I - V curve analyzed by a linear regression fit (straight line) and used to extract voltage-sensitive currents (*B*) by subtracting I_{Leak} from the total current. The voltage-sensitive inward current persisting after fast Na^+ current suppression showed further ramp-speed dependence, where the magnitude of the current was reduced by slower ramps (33 , 10 , and 3.3 mV/s , *B*). At the slowest ramp (3.3 mV/s), the current still failed to fully inactivate. *C* and *D*: ramp-speed dependency of magnitude and speed independence of voltage-dependent activation of g_{NaP} under Cd^{2+} ($200 \mu\text{M}$) and TEA (20 mM). The magnitude of g_{NaP} was calculated from current response similar to *B* and a Na^+ equilibrium potential of $+50 \text{ mV}$. Plateau of g_{NaP} is revealed near the depolarized voltage range (approximately -20 mV) after K^+ conductance block with TEA, with peak g_{NaP} that could exceed 4.5 nS (*C*, 70 mV/s ramp speed). Although g_{NaP} is attenuated as the voltage ramp speed is slowed (*C*, 70 to 6.7 mV/s), the voltage-dependent activation characteristics remained unchanged (*D*, normalized conductance and fitted with a Boltzmann sigmoid with $V_{1/2} = -37 \text{ mV}$ and $k = 4.9$).

under Ca^{2+} current blockade alone (Fig. 4*B*), multirate ramps revealed rate-dependent attenuation of the I_{NaP} , (with conductances as high as 4 – 5 nS at higher ramp speeds); essentially identical normalized conductance-voltage relationships were obtained at different ramp rates (Fig. 4*D*). A single Boltzmann curve could be fit to the set of normalized conductance-voltage relationships as illustrated in Fig. 4*D*, with $V_{1/2} = -37.4 \text{ mV}$ and $k = -4.9 \text{ mV}$, very similar to the values obtained for the other data sets described above.

The $g_{\text{NaP}}/g_{\text{Leak}}$ ratio differs between inspiratory neuron phenotypes

According to the model proposed by Butera et al. (1999a), bursting depends on dynamic interactions of g_{NaP} (which is voltage and time dependent) and the voltage-independent K^+ -dominated leak conductance g_{Leak} . Since the TTX-sensitive I_{NaP} was present in nonpacemaker as well as bursting-pacemaker neurons, we tested whether the ratio of g_{NaP} and g_{Leak} was correlated to the pacemaker behaviors. If either parameter is considered alone, inspiratory pacemaker and nonbursting cells are indistinguishable (Fig. 2, bottom). However, when both parameters are considered simultaneously and are plotted for individual cells in a plane with g_{NaP} and g_{Leak} on the ordinate and abscissa, respectively, the spatial relationship shown in Fig. 5 is obtained. Pacemaker cells ($n = 7$ analyzed) generally exhibited higher $g_{\text{NaP}}/g_{\text{Leak}}$ ratios than the sample of nonpacemaker neurons used for this analysis ($n = 10$).

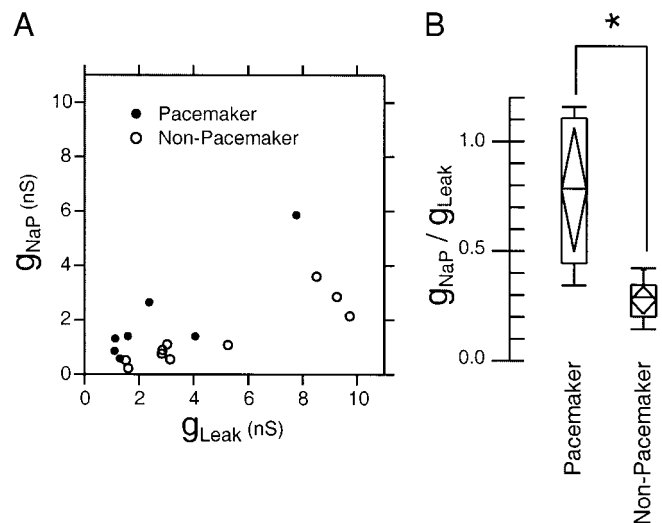


FIG. 5. *A*: plot of g_{NaP} vs. g_{Leak} indicating that pacemaker neurons generally have higher $g_{\text{NaP}}/g_{\text{Leak}}$ ratios than the nonpacemaker neurons tested. *B*: distributions of $g_{\text{NaP}}/g_{\text{Leak}}$ were significantly different between pacemaker and nonpacemaker groups ($P < 0.0002$, t -test). Box plots show the distribution extremes (horizontal bars), 25th and 75th percentiles (box height), and median (center bar); diamonds within box indicate parametric mean (center) and 95% confidence intervals (height); no vertical overlap between two diamonds indicates statistical difference with $\alpha = 0.05$ if data distributions are normally distributed, which is true for the present cases).

In each pacemaker and nonpacemaker group, $g_{\text{NaP}}/g_{\text{Leak}}$ ratios were distributed normally: 0.78 ± 0.31 (mean \pm SD) and 0.28 ± 0.03 , respectively. Deviation from a normal distribution was not significant in both groups: $P > 0.60$ and $P > 0.93$, respectively. The distributions of $g_{\text{NaP}}/g_{\text{Leak}}$ were significantly different between pacemaker and nonpacemaker groups: $P < 0.0002$ (Student's *t*-test). These data strongly suggested that pacemaker and nonpacemaker pre-BötC inspiratory neuron phenotypes were sampled from two distinct groups, each of which is normally distributed in terms of the $g_{\text{NaP}}/g_{\text{Leak}}$ ratios. We also used a Monte Carlo simulation (Manly 1991; Ripley 1981) to test whether the two phenotypes are spatially segregated in the $g_{\text{NaP}}-g_{\text{Leak}}$ plane (Fig. 5), to further confirm that these phenotypes comprised significantly different subsets of inspiratory cells based on the $g_{\text{NaP}}/g_{\text{Leak}}$ ratio. This analysis also showed that the relationship between bursting-pacemaker phenotype and the $g_{\text{NaP}}/g_{\text{Leak}}$ ratio is statistically significant at $P < 0.01$.

DISCUSSION

Membrane and electrophysiological properties of pre-BötC inspiratory neurons

We have analyzed electrophysiological properties of inspiratory cells in the pre-BötC in vitro and demonstrated the existence of a persistent Na^+ current with conductance values as high as 5 nS. These findings concur with our modeling studies (Butera et al. 1999a,b; Del Negro et al., 2001) that first postulated and demonstrated theoretically that I_{NaP} can function as a primary voltage-dependent burst-generating mechanism. We also confirmed previous studies (Del Negro et al. 2001; Johnson et al. 1994; Smith et al. 1991; Thoby-Brisson and Ramirez 2001) that inspiratory neurons can be divided into two phenotypes based on electrophysiological behaviors in the pre-BötC: bursting pacemaker-type and nonbursting inspiratory neurons. We analyzed a number of neuronal membrane and synaptic parameters that could contribute to or reflect these differences in cellular electrophysiological behavior. The sampled population revealed essentially no differences in properties such as R_{M} , I_{peak} , and Q_{syn} . Our sample included neurons in the upper 60 μm of the slice near the caudal end of the pre-BötC—the region available to probing with neuron visualization-based methods for patch clamping (IR-DIC and IR-DIC combined with Ca^{2+} fluorescence imaging of cell activity). There have been no previous studies of membrane and synaptic properties of pre-BötC inspiratory neurons to quantify heterogeneity and to compare bursting pacemaker and nonbursting cell types. An important finding with our sampled population was that all identified inspiratory neurons expressed a range of I_{NaP} and the principal distinguishing property for the bursting pacemaker versus nonpacemaker behaviors was the $g_{\text{NaP}}/g_{\text{Leak}}$ ratios, which, as further discussed in the following text, reflects the basic biophysical mechanism for bursting.

I_{NaP} and bursting pacemaker behavior of pre-BötC inspiratory neurons

VOLTAGE-DEPENDENT ACTIVATION OF I_{NaP} . In many invertebrate and mammalian bursting neurons, the onset of bursting is caused by a subthreshold-activating inward cationic current. This current is responsible for maintaining the negative-slope

region of the *I-V* curve in the subthreshold voltage range. Although Ca^{2+} imaging studies indicate that pre-BötC bursting pacemaker neurons have Ca^{2+} currents (Koshiya and Smith 1999a), bursting persists under low Ca^{2+} conditions and accordingly we have proposed that I_{NaP} is the primary candidate mechanism for oscillatory burst generation (Butera et al. 1999a). Our data indicate that I_{NaP} in pre-BötC inspiratory neurons is TTX sensitive and activates at subthreshold potentials near -60 mV with a $V_{1/2}$ of approximately -40 mV. Errors in our estimates of the activation parameters could arise from voltage clamp errors due to inadequate space clamp and contamination of the measured inward current due to incomplete inactivation of the transient fast-activating, action-potential generating Na^+ current at the slow voltage ramp speeds used for our analysis. Furthermore, in cases in which K^+ currents were not blocked with TEA, the voltage-dependent outward K^+ currents can distort the shape of the ramp *I-V* curve and reduce the amplitude of the measured inward current, although the Boltzmann function fits for the inward current activation were essentially identical with and without TEA. On the other hand, our *I-V* plots are consistent in shape with other *I-V* characteristics estimated by slow voltage ramps: 2.33 to 70 mV/s (Fleidervish and Gutnick 1996). When using ramps of ≥ 35 mV/s, Fleidervish and Gutnick (1996) reported that I_{NaP} begins to activate around -60 mV and reaches a peak by -25 mV, similar to our data. Furthermore, our values of $V_{1/2}$ and k are essentially identical to the values used in our minimal pacemaker cell model (Butera et al. 1999a), which produces voltage-dependent bursting that closely mimics the experimentally observed behavior (Del Negro et al. 2001) when I_{NaP} interacts dynamically with the K^+ -dominated leakage conductance (see following text). Moreover, voltage-dependent bursting similar to that observed experimentally for pre-BötC neurons and predicted by our model can be produced by using the dynamic clamp to artificially incorporate in neurons I_{NaP} with the voltage dependence of activation that we have modeled and found experimentally (Butera et al. 2001).

Currently we do not have information on the origin of the persistent current at the channel level in the inspiratory neurons studied. A type of persistent Na^+ current in isolated cells has been attributed entirely to “modal gating” and late channel openings of the same Na^+ channels that are responsible for the fast transient Na^+ current generating action potentials (Alzheimer et al. 1993). TTX-sensitive persistent Na^+ current has also been proposed to originate from subthreshold gating of the fast transient current in isolated tuberomammillary neurons (Tadde and Bean, 2002), implying that complex electrophysiological properties including pacemaker behavior arising from a persistent Na^+ current could result from voltage-dependent gating properties of a single ubiquitous Na^+ channel type. Regardless of the molecular mechanism, inspiratory cells have a persistent inward Na^+ current that activates in the subthreshold voltage range to support voltage-dependent oscillatory bursting.

INACTIVATION PROPERTIES OF I_{NaP} . We have not yet quantified the voltage dependence of steady-state inactivation nor the inactivation time constants of I_{NaP} in pre-BötC inspiratory neurons. This information is important for understanding mechanisms of burst termination and the dynamics of the oscillatory bursting cycle. As shown by the present data and

our previous modeling studies, initiation and termination of bursting are accompanied by a rapid transition between the silent phase and the subthreshold depolarization with firing of action potentials and vice versa. From theoretical studies of mechanisms generating oscillatory bursting behavior, a minimal mechanism for bursting requires a slow recovery process, such as a slow voltage-dependent conductance inactivation mechanism. In our minimal models of pre-BötC pacemaker neurons, we concluded that this process is more likely related to slow inactivation of I_{NaP} rather than slow activation of an outward K^+ current, which would interact with a noninactivating I_{NaP} for burst termination. In the model, I_{NaP} inactivation during a burst contributes to burst termination and the slow kinetics of recovery from inactivation controls the time course of the quiescent interburst interval. Slow voltage-dependent inactivation kinetics (on the order of seconds) are required to produce the bursting dynamics observed for the pre-BötC pacemaker cells. In the present experiments, the attenuation of the peak inward current that we observed as voltage-clamp ramp speed is reduced and the shape of the I - V relationships obtained experimentally is consistent with the kinetics/voltage-dependent time constants of I_{NaP} inactivation of our model. Simulations with voltage ramps show the reduction of the peak I_{NaP} by over 50% as ramp speed decreases over the range of speeds used in our experimental protocols but persistence of the inward current at the lowest ramp speeds (3.3 mV/s) used due to very slow inactivation (R. J. Butera, unpublished observations). Fleidervish and Gutnick (1996) demonstrated a TTX-sensitive I_{NaP} in rodent neocortical neurons and reported the time constant for the onset of slow inactivation of I_{NaP} was approximately 2 s at +20 mV and the time constant for recovery from slow inactivation of 2.3 s at -70 mV, which are consistent with the values employed in our model (2–10 s) (Butera et al. 1999a).

Heterogeneity of subthreshold conductances

We found evidence for I_{NaP} in both inspiratory neuron phenotypes (bursting pacemaker and nonbursting) in the pre-BötC. In our sample populations, we did not detect differences in the voltage dependence of activation, suggesting that the current was identical (although we did not analyze the voltage ramp-speed dependence of the peak I_{NaP} in nonbursting cells). While the activation properties of I_{NaP} appeared identical, there was considerable heterogeneity in the peak inward current densities (measured at voltage-clamp ramp speeds of 30 mV/s) within each population. For pacemaker type neurons the current densities were 4.3 ± 2.2 versus 2.0 ± 0.4 pA/pF in nonpacemaker cells. We also found heterogeneity in the values of leak conductance. Similarly we have previously found (Del Negro et al. 2001) heterogeneity in bursting behavior of inspiratory pacemaker cells that theoretically would reflect cell-to-cell differences in current densities (Butera et al. 1999b). Our pacemaker network model of the pre-BötC kernel indicates that such heterogeneity in g_{NaP} and g_{Leak} is functionally important because it extends the dynamic range for population burst frequency control: robust synchronous bursting occurs across a much greater range of parameter space in terms of the range of depolarizing inputs that control neuron voltage-dependent bursting and regulate population burst frequency (Butera et al. 1999b).

Determinants of bursting pacemaker behavior

Our model of the pre-BötC kernel postulates that voltage-dependent oscillatory bursting arises in a subset of rhythm-generating cells that express critical levels of g_{NaP} in relation to g_{Leak} (Butera et al. 1999b). Bursting behavior at the cellular level depends on dynamic interactions of the whole-cell currents mediated by these two key conductances (Butera et al. 1999a). A large g_{NaP} will produce a steeper negative slope in the whole-cell I - V relationship that gives rise to bursting behavior and will result in a larger $g_{\text{NaP}}/g_{\text{Leak}}$ ratio for bursting pacemaker versus nonbursting neurons as illustrated in Fig. 5. Accordingly we also analyzed g_{Leak} , which our data indicate is not voltage sensitive, as postulated in the model, and we analyzed the relationships between g_{NaP} versus g_{Leak} . The graphical form of the g_{NaP} versus g_{Leak} plot roughly resembles a pie wedge, in which bursting-pacemaker activity emerges for a set of $g_{\text{NaP}}/g_{\text{Leak}}$ combinations. Cells do not exhibit oscillatory bursting behavior with $g_{\text{NaP}}/g_{\text{Leak}}$ ratios lower than those within the parameter regime for bursting. This pie wedge-shaped graph is theoretically predicted for our model inspiratory pacemaker neurons. In Fig. 6, we have plotted the graph of g_{NaP} versus g_{Leak} from pacemaker neuron model 1 of Butera et al. (1999a). This graph emphasizes that there are three intrinsic activity states of neurons determined by the $g_{\text{NaP}}/g_{\text{Leak}}$ ratio: silent, oscillatory bursting, and beating (tonic spiking), for which bursting behavior only occurs for a finite set of $g_{\text{NaP}}/g_{\text{Leak}}$ combinations. Taken together, our experimental and theoretical data suggest that the empirical distribution of bursting-pacemaker and nonpacemaker cells depends on the ratio of g_{NaP} and g_{Leak} , and the dynamic interaction of g_{NaP} and g_{Leak} can control the expression of these behaviors (Butera et al. 1999a; Del Negro et al. 2001).

Thus the present results suggest that bursting pacemaker versus nonbursting behaviors can be distinguished by the $g_{\text{NaP}}/g_{\text{Leak}}$ ratio as in the minimal model of Butera et al. (1999a), even though the cells may have other subthreshold-activating conductances, such as transient outward currents, voltage-activated calcium currents, and hyperpolarization-acti-

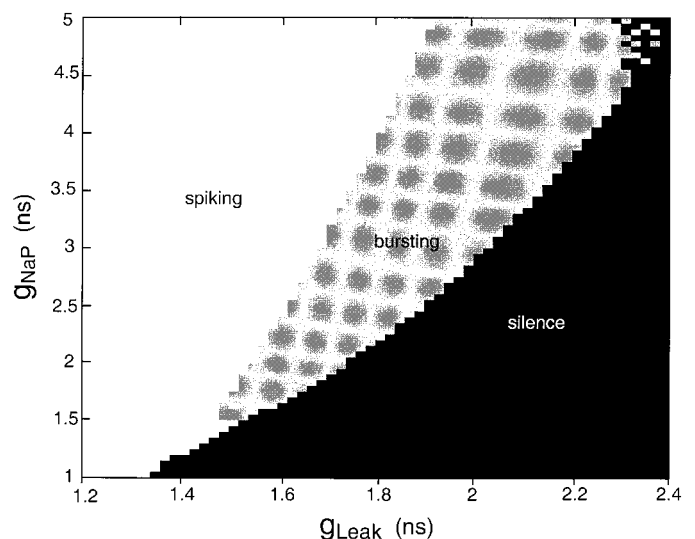


FIG. 6. Intrinsic modes of pacemaker cell activity of Butera et al.'s (1999a) inspiratory pacemaker model 1 as a function of g_{NaP} and g_{Leak} . This plot illustrates that pacemaker bursting occurs within a range of $g_{\text{NaP}}/g_{\text{Leak}}$ parameter ratios that form a wedge-shaped region in the $g_{\text{NaP}}-g_{\text{Leak}}$ plane.

vated mixed-cationic currents (Thoby-Brisson et al. 2000), which could contribute to the neuronal dynamic behavior. The dynamics of bursting reflects a complex interaction of multiple currents and even high-voltage-activated currents such as the delayed rectifier K^+ current can affect bursting behavior. In Butera et al.'s (1999a) simulations with model 1, for example, subthreshold oscillations can exist even if the fast, transient action potential-generating Na^+ current is removed, but their period is slightly different, suggesting that the dynamics of the delayed rectifier K^+ current may play a minor role in determining bursting properties such as burst duration. Nevertheless, the present results indicate that the core biophysical mechanism for rhythmic bursting in the pre-BötC inspiratory neurons expressing I_{NaP} is the dynamic interaction of I_{NaP} and I_{Leak} as postulated by the models of Butera et al. (1999a).

We currently do not know the precise functional roles of the experimentally sampled inspiratory cells in rhythm generation with the pre-BötC network. The pre-BötC has a heterogeneous cellular composition, for which only a subpopulation of the excitatory interneurons may actually be responsible for generating the rhythm. According to our models that incorporate a heterogeneous distribution of g_{NaP} and g_{Leak} , many of the neurons may not actually be burst capable due to low g_{NaP}/g_{Leak} ratios; these neurons nonetheless can participate in generation of the population-level inspiratory burst through excitatory synaptic activity. Indeed our simulations (Butera et al. 1999b) show that synchronized rhythms can emerge at the population level when there is a mixture of burst-capable and nonburst-capable neurons with a very high fraction of nonburst capable neurons, as well as under conditions with low g_{NaP}/g_{Leak} ratios where none of the neurons in the rhythm-generating kernel express voltage-dependent bursting pacemaker behavior. Moreover, a recent report suggests that the voltage-dependent bursting mediated by I_{NaP} may not be necessary for rhythm generation (Del Negro et al. 2002), requiring further experimental clarification of the role of voltage-dependent pacemaker bursting engendered at the cellular level by I_{NaP} . Nevertheless, I_{NaP} is a common property of pre-BötC inspiratory neurons. A similar conclusion that I_{NaP} is a widespread property has been reached by McCrimmon et al. (2001) who have identified a TTX-sensitive I_{NaP} in many neurons dissociated in culture from the pre-BötC and neighboring reticular formation, although their neurons were not functionally identified as inspiratory cells. I_{NaP} may be particularly important because it endows cells with a subthreshold-activating inward current that can amplify synaptic drive, promoting synchronization of neuronal activity in the network that, combined with the tendency for intrinsic bursting in a subset of cells, leads to the emergence of population-level bursting (Butera et al. 1999b) and network rhythms.

REFERENCES

- ALZHEIMER C, SCHWINDT PC, AND CRILL WE. Modal gating of Na^+ channels as a mechanism of persistent Na^+ current in pyramidal neurons from rat and cat sensorimotor cortex. *J Neurosci* 13: 660–673, 1993.
- BUTERA RJ, JR., RINZEL J, AND SMITH JC. Models of respiratory rhythm generation in the pre-Bötzing complex. I. Bursting pacemaker neurons. *J Neurophysiol* 81: 382–397, 1999a.
- BUTERA RJ, JR., RINZEL J, AND SMITH JC. Models of respiratory rhythm generation in the pre-Bötzing complex. II. Populations of coupled pacemaker neurons. *J Neurophysiol* 81: 398–415, 1999b.
- BUTERA RJ, WILSON CG, DEL NEGRO CA, AND SMITH JC. A methodology for achieving high-speed rates for artificial conductance injection in electrically excitable biological cells. *IEEE Trans Biomed Eng* 48: 1460–1470, 2001.
- DEL NEGRO CA, JOHNSON SM, BUTERA RJ, AND SMITH JC. Models of respiratory rhythm generation in the pre-Bötzing complex. III. Experimental tests of model predictions. *J Neurophysiol* 86: 59–74, 2001.
- DEL NEGRO CA, MORGADO-VALLE C, AND FELDMAN JL. Respiratory rhythm: an emergent network property? *Neuron* 34: 821–830, 2002.
- EDWARDS FA, KONNERTH A, SAKMANN B, AND TAKAHASHI T. A thin slice preparation for patch clamp recordings from neurones of the mammalian central nervous system. *Pflügers Arch* 414: 600–612, 1989.
- FELDMAN JL AND SMITH JC. Cellular mechanisms underlying modulation of breathing pattern in mammals. *Ann NY Acad Sci* 563: 114–130, 1989.
- FLEIDERVISH IA AND GUTNICK MJ. Kinetics of slow inactivation of persistent sodium current in layer V neurons of mouse neocortical slices. *J Neurophysiol* 76: 2125–2129, 1996.
- GRAY PA, JANCZEWSKI WA, MELLE N, MCCRIMMON DR, AND FELDMAN JL. Normal breathing requires preBotzinger complex neurokinin-1 receptor-expressing neurons. *Nature Neurosci* 4: 927–930, 2001.
- GRAY PA, REKLING JC, BOCCHIARO CM, AND FELDMAN JL. Modulation of respiratory frequency by peptidergic input to rhythmogenic neurons in the preBotzinger complex. *Science* 286: 1566–1568, 1999.
- JOHNSON SM, SMITH JC, FUNK GD, AND FELDMAN JL. Pacemaker behavior of respiratory neurons in medullary slices from neonatal rat. *J Neurophysiol* 72: 2598–2608, 1994.
- KOSHIYA N, DEL NEGRO C, BUTERA RJ, AND SMITH JC. Persistent sodium current (I_{NaP}) in pre-Bötzing complex (pre-BötC) inspiratory neurons. *Soc Neurosci Abstr* 27: 243.3, 2001.
- KOSHIYA N AND GUYENET PG. Tonic sympathetic chemoreflex after blockade of respiratory rhythmogenesis in the rat. *J Physiol (Lond)* 491: 859–869, 1996.
- KOSHIYA N AND SMITH JC. Neuronal pacemaker for breathing visualized in vitro. *Nature* 400: 360–363, 1999a.
- KOSHIYA N AND SMITH JC. Subthreshold-activating persistent sodium conductance (g_{NaP}) in inspiratory neurons of the pre-Bötzing complex in vitro. *Soc Neurosci Abstr* 25: 696, 1999b.
- MANLY BFJ. *Randomization and Monte Carlo Methods in Biology*. London: Chapman and Hall, 1991.
- MCCRIMMON DR, MONNIER A, PTAK K, ZUMMO G, ZHANG Z, AND ALHEID GF. Respiratory rhythm generation: preBotzinger neuron discharge patterns and persistent sodium current. In: *Frontiers in Modeling and Control of Breathing*, edited by Poon C-S and Kazemi H. New York: Plenum, 2001, p.147–152.
- RAMIREZ JM, SCHWARZACHER SW, PIERREFICHE O, OLIVERA BM, AND RICHTER DW. Selective lesioning of the cat pre-Bötzing complex *in vivo* eliminates breathing but not gasping. *J Physiol (Lond)* 507: 895–907, 1998.
- REKLING JC AND FELDMAN JL. PreBotzinger complex and pacemaker neurons: hypothesized site and kernel for respiratory rhythm generation. *Annu Rev Physiol* 60: 385–405, 1998.
- RIPLEY BD. *Spatial Statistics*. New York: Wiley, 1981.
- SMITH JC, BUTERA RJ, KOSHIYA N, DEL NEGRO CA, WILSON CG, AND JOHNSON SM. Respiratory rhythm generation in neonatal and adult mammals: the hybrid pacemaker-network model. *Respir Physiol* 122: 131–147, 2000.
- SMITH JC, ELLENBERGER HH, BALLANYI K, RICHTER DW, AND FELDMAN JL. Pre-Bötzing complex: a brainstem region that may generate respiratory rhythm in mammals. *Science* 254: 726–729, 1991.
- TADDESE A AND BEAN BP. Subthreshold sodium current from rapidly inactivating sodium channels drives spontaneous firing of tuberomammillary neurons. *Neuron* 33: 587–600, 2002.
- THOBY-BRISSON M AND RAMIREZ JM. Identification of two types of inspiratory pacemaker neurons in the isolated respiratory neural network of mice. *J Neurophysiol* 86: 104–112, 2001.
- THOBY-BRISSON M, TELGKAMP P, AND RAMIREZ JM. The role of the hyperpolarization-activated current in modulating rhythmic activity in the isolated respiratory network of mice. *J Neurosci* 20: 2994–3005, 2000.